Chapter I.3
Principles of Aerosol LIDAR Systems

Vincenzo Rizi and Marco Iarlori

1 Introduction

This lecture is dedicated to the description of the fundamentals of the aerosol lidar theory (of course it is not a complete overview!).

I will talk about aerosol LIDAR technique, discussing a kind of classical representation of the LIDAR technique; in other words: monitoring the fate of coherent and undistinguishable photons travelling in and interacting with a non-homogeneous medium: atmosphere (including aerosols).

Hopefully, it will be clear, along this lecture, how LIDAR can measure some fundamental aerosol optical properties; in this context I will try to connect to other lectures.

I will try to keep alive your attention presenting the architecture of LIDAR instruments (i.e., UV/Visible – Rayleigh/Mie and Raman LIDARs), which are mainly devoted to aerosol observations. Using, in real time, our own software, I will also discuss the down- and upsizing of the different lidar components (lasers, telescopes, detectors) for the best observational strategy of the various atmospheric aerosols (including clouds).

Maybe exaggerating and upon my ability, the expected outcomes are the following. You will be able to:

- understand how LIDAR techniques are used to characterize atmospheric aerosols,
- perform tradeoffs among the engineering parameters of a LIDAR system to achieve a given measurement capability, and
- evaluate the performance of LIDAR systems.

V. Rizi (✉)
CETEMPS/Dipartimento di Fisica, Università Degli Studi dell'Aquila, L'Aquila, Italy
e-mail: Vincenzo.Rizi@aquila.infn.it

Presented at International Summer School on Atmospheric and Oceanic Sciences, L'Aquila, Italy, 3–7 September 2007

D. Cimini et al. (eds.), *Integrated Ground-Based Observing Systems*,
DOI 10.1007/978-3-642-12968-1_3,

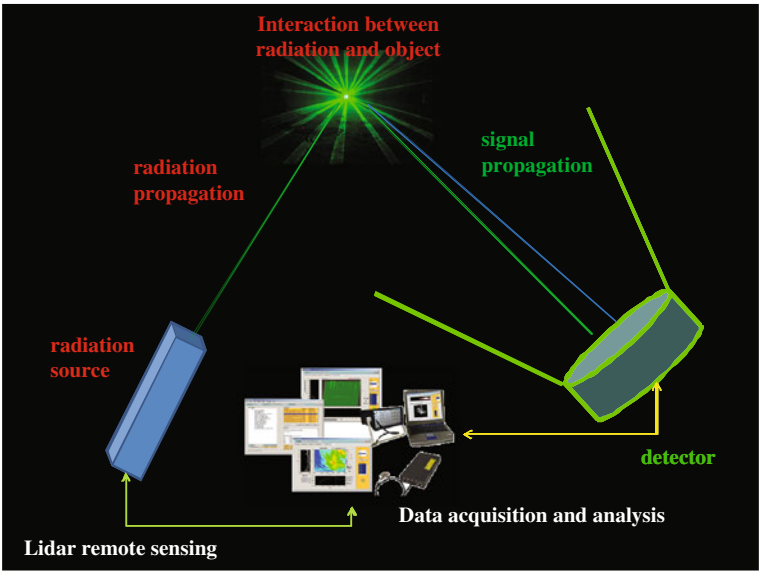

Fig. I.3.1 Layout of a lidar system

The lidar layout in Fig. I.3.1 is typical: the generated radiation (a laser pulse) propagates in the medium (the atmosphere), interacts with the medium, and propagates back to the detector (telescope). All is driven by instrumentations that set the timescale of the radiation travel, or the range from where the signal returns back (carrying information concerning the interaction with the medium and its components).

A short history of the lidar technique: searchlight technique, very similar to the modern lidar technique, has been used for aerosol observations (Hulburt, 1937); Johnson et al. (1939) and Tuve et al. (1935) modulated the searchlight beam with a mechanical shutter, increasing the sensitivity of technique; Elterman (1951) has used searchlight technique to study stratosphere. After the laser technology became widely available, the lidar started to be a fundamental instrument for the atmospheric aerosol observations. The first (ruby) laser was invented in 1960 (Schawlow and Townes, 1958; Maiman, 1960); laser pulse technique (Q-Switch) (McClung and Hellwarth, 1962) constituted another fundamental step. The first laser studies of the atmosphere were undertaken by Fiocco and Smullin (1963) for upper region and by Ligda [1963] for troposphere. The indicated papers are very interesting, and after reading, my personal feeling is that we (lidar people) are playing with well-proofed toys.

2 Lidar Architecture

In the next slides, I will give more details and highlights about the lidar components: transmitter, receiver, system control, and data acquisition (Fig. I.3.2).

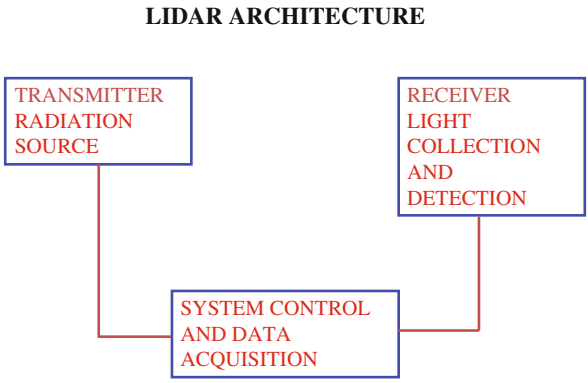

Fig. I.3.2 Lidar architecture

2.1 Transmitter

It provides laser pulses (Fig. I.3.3) that meet certain requirements depending on application needs (e.g., wavelength, pulse duration, pulse energy, repetition rate, divergence angle). Transmitter consists of lasers, collimating and steering optics, and diagnostic equipment (for checking the laser stability, etc.).

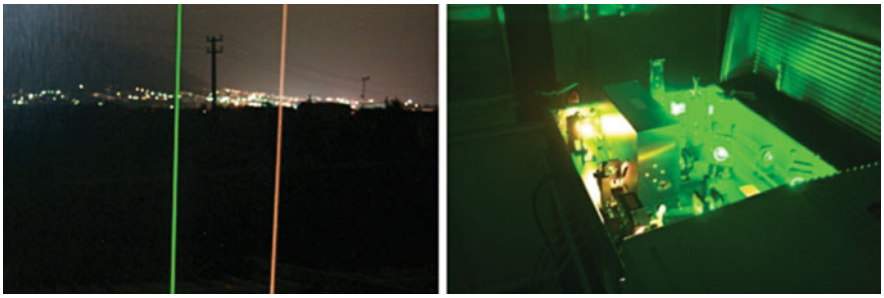

Fig. I.3.3 Laser and laser beams

2.2 Receiver

It collects and detects returned photons, It consists of telescopes, optical filters, collimating optics, photon detectors, and fast electronics, etc. (Fig. I.3.4). The receiver can spectrally distinguish the returned photons.

2.3 System Control and Data Acquisition

It records returned data and corresponding time of flight and provides the coordination to transmitter and receiver. It consists of multi-channel scaler which has very precise clock, discriminator, computer, and software (Fig. I.3.5).

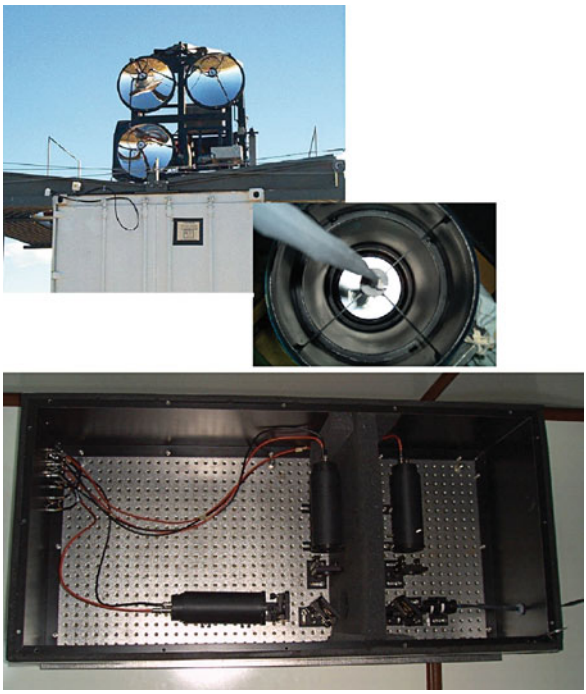

Fig. I.3.4 Telescopes and detectors

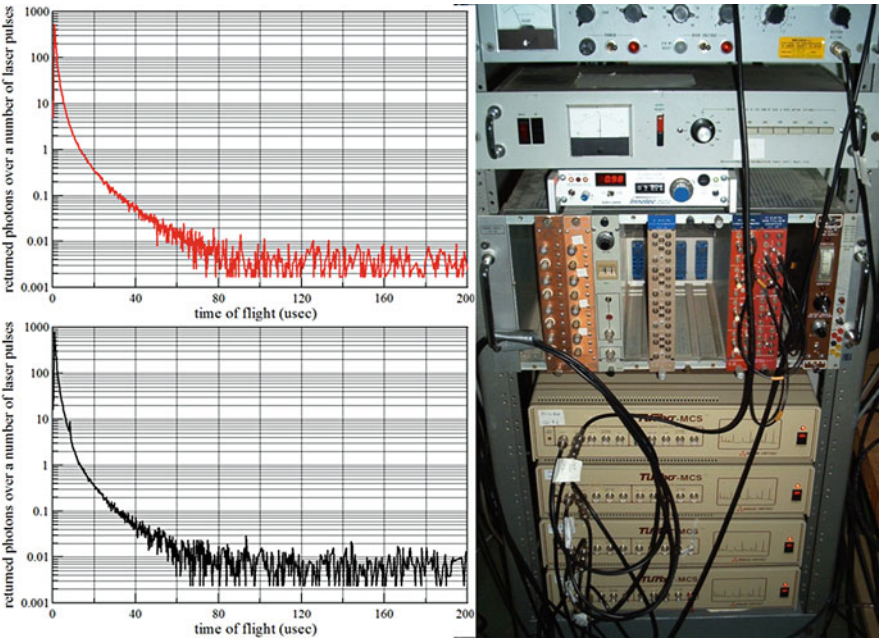

Fig. I.3.5 Lidar electronics and recorded signals

2.4 Lidar Return

Then the typical lidar return appears like in Fig. I.3.6. A number of photons collected as a function of the flight time/range. The question is: which kind of information (focusing on aerosols) is carried back by the detected photons?

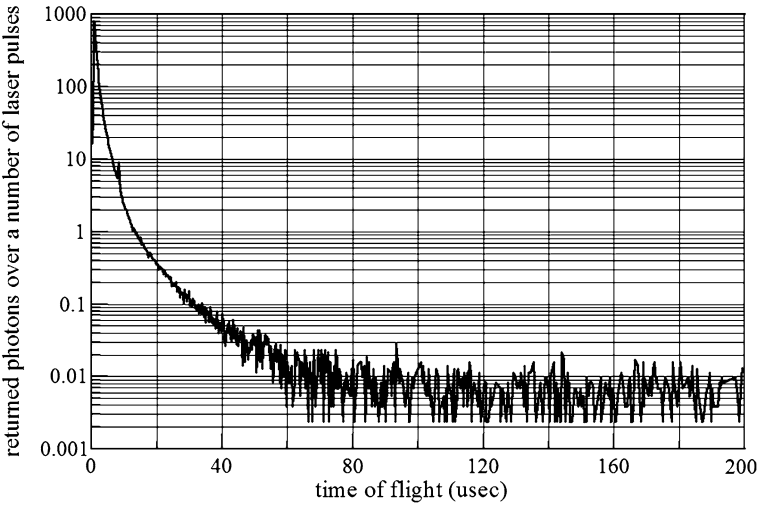

Fig. I.3.6 Lidar return: number of photons vs. flight time

3 Lidar Equation

The description of lidar returns is done setting up the right equation: the lidar equation relates the received photon counts with the transmitted laser photons, the light transmission in atmosphere or medium, the physical interaction between light and objects, the photon receiving probability, and the lidar system efficiency and geometry.

The lidar equation is based on the physical picture of lidar remote sensing and derived under two assumptions: only independent and single scattering processes. Different lidars may use different forms of the lidar equation, but all come from the same picture. I will limit my discussion to the UV-Visible wavelength lidars.

Let us introduce some notation. In general, the interaction between the light photons and the particles is a scattering process.

The expected photon counts are proportional to the product of the

- number of transmitted laser photons,
- probability that a transmitted photon is scattered,
- probability that a scattered photon is collected,

- light transmission through medium, and
- overall system efficiency.

Background photon counts and detector noise also contribute to the expected photon counts. The number of collected photons in a time interval Δt (from range interval between s and $s + \Delta s$, where $\Delta s = c \cdot \Delta t/2$, c is the speed of light) is

$$N_S(\lambda_o, \lambda, R) = N_o(\lambda_o)T(\lambda_o, s)[\beta(\lambda_o, \lambda, s)\Delta s]T(\lambda, s)\frac{d\Omega}{4\pi}\eta(\lambda, \lambda_o)G(s) + N_B, \quad (1)$$

where

$N_o(\lambda_o)$	number of emitted photons
$T(\lambda_o, s)$	laser transmission through the medium
$\beta(\lambda, \lambda_o, s) \cdot \Delta s$	probability of a transmitted photon to be scattered
$T(\lambda, s)$	scattered photon transmission through the medium
$d\Omega/4\pi$	probability of a scattered photon to be collected
$\eta(\lambda, \lambda_o)G(s)$	lidar system efficiency and geometry factor

3.1 Transmitter Laser Photons

From the datasheet of a standard 355-nm pulsed laser (4 mW output power, few micro Joules per pulse), it is possible to evaluate the number of the photons emitted per laser pulse: for the above laser's specifications it is about 6.7×10^{12} photon per pulse.

3.2 Transmission

It accounts for the processes that could extinguish the travelling photons; it can be interpreted as the relative fraction of propagating photons that travel a distance without interacting. About the interacting photons I will say more in the next paragraphs.

$$T(\lambda, s) = T^{\lambda}_{\text{mol}}(s) \cdot T^{\lambda}_{\text{aer}}(s) \cdot T^{\lambda}_{\text{abs}}(s),$$

where $T^{\lambda}_{\text{mol}}(s)$, molecular scattering transmission; $T^{\lambda}_{\text{aer}}(s)$, aerosol scattering transmission; $T^{\lambda}_{\text{abs}}(s)$, gas absorption transmission; and

$$T^{\lambda}_{\text{mol}}(s) = \exp\left(-\int_0^s \sigma^{\lambda}_{\text{mol}} n_{\text{mol}}(s)ds\right)$$

$$T^{\lambda}_{\text{aer}}(s) = \exp\left(-\int_0^s \left[\int_0^{\infty} dr\pi r^2 Q_{\text{ext}}(r, m, \lambda)n_{\text{aer}}(s, r)\right] ds\right)$$

$$T^{\lambda}_{\text{abs}}(s) = \exp\left(-\sum_i \int_0^s \sigma^{i}_{\text{abs}}(\lambda)n^{i}_{\text{abs}}(s)ds\right)$$

where n_{mol}, atmospheric molecular number density; n_{aer}, aerosol size distribution; n^i_{abs}, ith absorbing gas number density; $\sigma^{\lambda}_{\mathrm{mol}}$, molecular scattering total cross section; $Q_{\mathrm{ext}}(r, m, \lambda)$, Mie scattering extinction efficiency of an aerosol particle (r, radius; m, index of refraction); $\sigma^i_{\mathrm{abs}}(\lambda)$, ith gas absorbing cross section.

3.3 Backscattering

The volume backscattering coefficient is the probability per unit distance travel that a photon is backscattered (per unit of solid angle) or scattered in the direction of the receiver:

$$\beta(\lambda_o, \lambda, s) = \sum_i \frac{d\sigma_i(\lambda_o, \lambda)}{d\Omega} n_i(s).$$

If the scattering objects are aerosols,

$$\beta^{\lambda}_{\mathrm{aer}}(s) = \frac{1}{4\pi} \int_0^{\infty} dr \cdot \pi r^2 \cdot Q_{\mathrm{bck}}(r, m, \lambda) \cdot n_{\mathrm{aer}}(s, r),$$

where $n_{\mathrm{aer}}(s, r)$, aerosol size distribution and $Q_{\mathrm{bck}}(r, m, \lambda)$, Mie backscattering efficiency of an aerosol particle (r, radius; m, index of refraction).

3.4 Geometrical Collecting Efficiency

This is the probability that a scattered photon is collected by the receiving telescope.

$$\frac{d\Omega}{4\pi} = \frac{A}{s^2}$$

Note that this is proportional to the collecting area, and it depends on the range from where the light is collected (Fig. I.3.7).

3.5 Optical Collecting Efficiencies

Some of these effects are due to the optical setup and optics performances. In the receiver there are filters to discriminate, according to the wavelength, the collected photons [$\eta(\lambda, \lambda_o)$]. In addition the receiving telescope can introduce a geometrical form factor that modulates the collecting efficiency as a function of range, $G(s)$ (Fig. I.3.8).

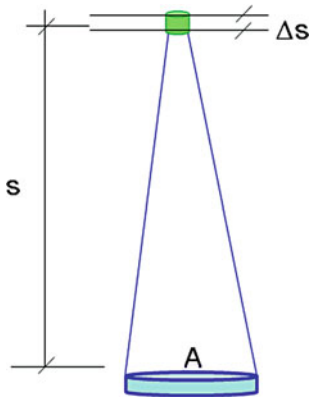

Fig. I.3.7 Receiver field of view

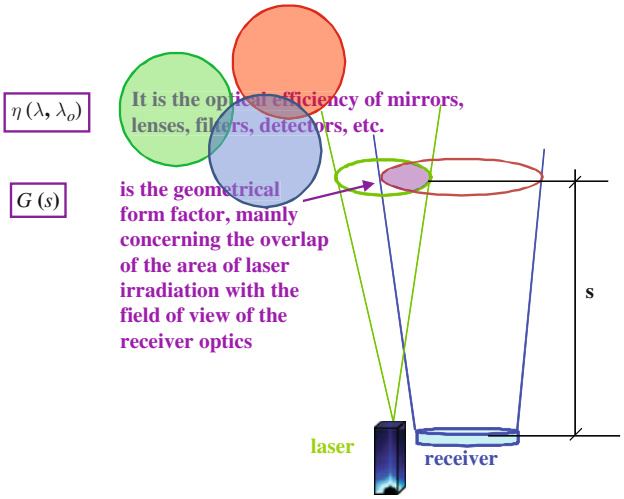

Fig. I.3.8 Schematic of optical collecting efficiency

3.6 Noise

The better one (always mixed up with more subtle noises) is linear, range independent, and white (sky light and detector/electronic noise).

4 Different Forms of Lidar Equation

Lidar equation may change forms to represent each particular physical process (Mie, Rayleigh and Raman scattering, etc.) and lidar application.

Going further into the physical processes (hopefully, I am still discussing what I have promised), let us take a break. I will show a funny representation of the lidar processes.

4.1 A Physics-ological Drama

The cartoon animation presented in Figs. I.3.9–I.3.13 is available upon request to vincenzo.rizi@aquila.infn.it.

SCENE I The laser emission
SCENE II The upward travel

In which photons make different experiences at the beginnings of the travel, several of them will be lost (extinction).

SCENE III Local backscattering

Some lucky guys find the way back, with unchanged identities (aerosol and molecular elastic backscattering) or quite evident differences (depending on the encountered situations, molecular Raman backscattering)

SCENE IV The downward travel

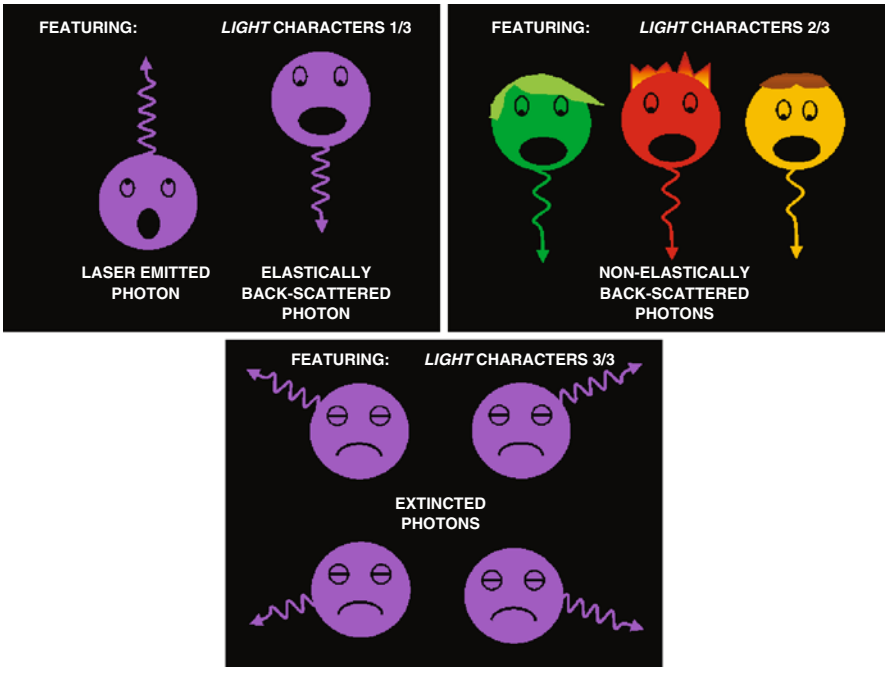

Fig. I.3.9 The cartoon representation of fundamental lidar processes: the main characters

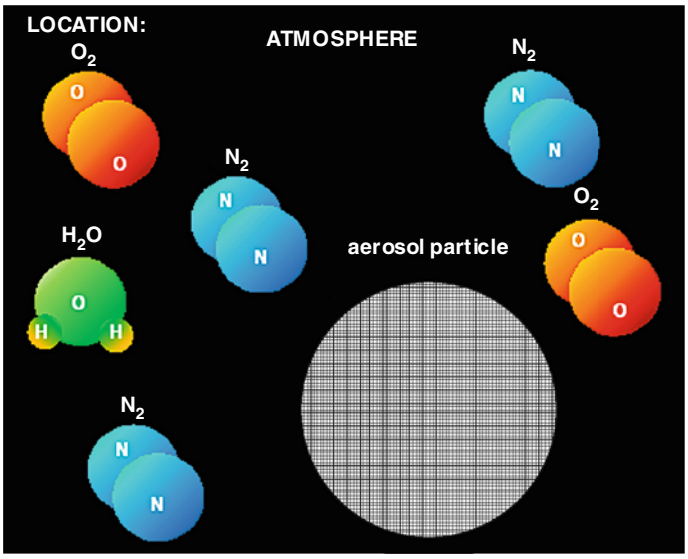

Fig. I.3.10 The cartoon representation of fundamental lidar processes: the location (the atmosphere)

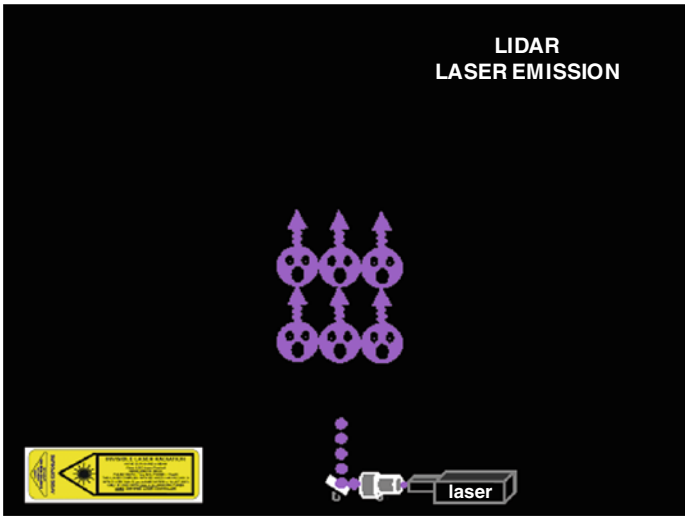

Fig. I.3.11 The cartoon representation of fundamental lidar processes: leaving together . . .

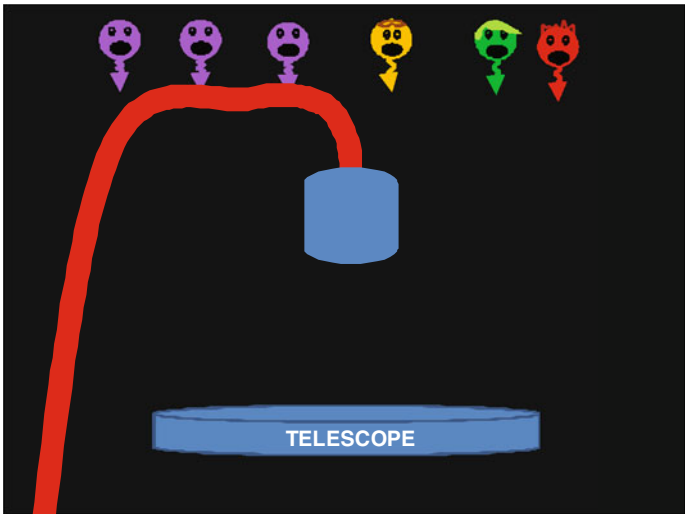

Fig. I.3.12 The cartoon representation of fundamental lidar processes: at home, carrying different information . . .

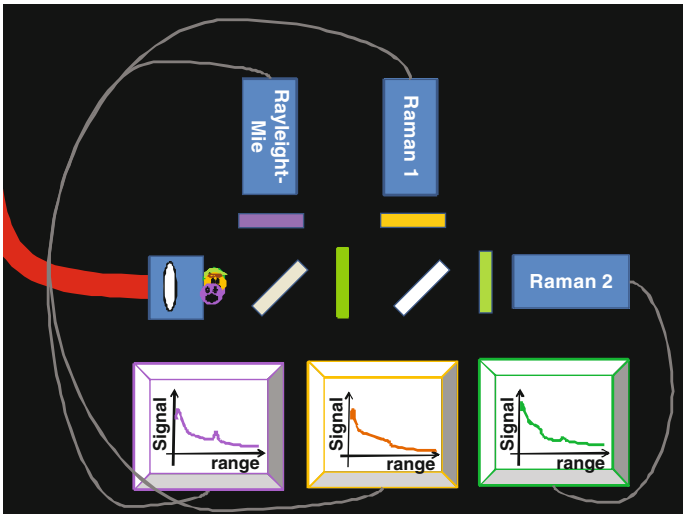

Fig. I.3.13 The cartoon representation of fundamental lidar processes: communicating all the stories (something useful remains): what they have done, where they have travelled

On the way back . . . not fully unexpected losses

SCENE V Detection
SCENE VI

5 Lidar Physical Processes

Then, there are many physical processes involved when the lidar light propagates and interacts in the atmosphere:

- Scattering (elastic and inelastic): Mie, Rayleigh, Raman
- Absorption and differential absorption
- Resonant fluorescence
- Doppler shift and Doppler broadening
- . . .

I will discuss only the scattering processes; before starting let us introduce some additional definitions. Light propagation in atmosphere relies on transmission/extinction, where: Extinction = Scattering + Absorption, and the scattering processes could be elastic and inelastic.

5.1 Rayleigh Scattering

Rayleigh scattering is referred to the *elastic scattering* from atmospheric molecules (particle size is much smaller than the wavelength), i.e., scattering with no apparent change of wavelength, although still undergoing Doppler broadening and Doppler shift. However, depending on the resolution of detection, Rayleigh scattering consists of the Cabannes scattering (really elastic scattering from molecules) and pure rotational Raman scattering.

5.2 Raman Scattering

Raman scattering is the *inelastic scattering* with rotational quantum state or vibration-rotational quantum state change as a result of scattering. The Raman scattered photons are shifted in wavelength, this shift is the signature of the stationary energy levels of the irradiated molecule. The Raman spectroscopy in a gas mixture identifies and measures the different components. Example: the nitrogen and oxygen molecules show Raman shifts (roto-vibrational transitions) of 2,327 cm^{-1} and 1 556 cm^{-1}, respectively.

5.3 Mie Scattering for the Other Object (Aerosol) in the Atmosphere

Mie scattering is the *elastic scattering* from spherical particles (Mie, 1908), which includes the solution of Rayleigh scattering. However, in lidar field, first, Mie scattering is referred to the elastic scattering from spherical particles whose size is comparable to or larger than the wavelength. Furthermore, Mie scattering is generalized to elastic scattering from overall aerosol particles and cloud droplets, i.e., including non-spherical particles.

5.4 Lidar Backscattering and Extinction

A lidar is designed to observe the atmospheric backscattering and the extinction; we will concentrate on the systems which are able to sample the aerosol backscattering and extinction.

Physical process	Back-scattering cross section
Mie (aerosol) scattering	$10^{-8} \div 10^{-10}$ **cm**^{2} **sr**$^{-1}$
Rayleigh scattering	10^{-27}**cm**^{2} **sr**$^{-1}$
Raman scattering	10^{-30}**cm**^{2} **sr**$^{-1}$

The numbers in the table give an idea of the magnitude of the different scattering processes. Note how small is the effect of the Raman scattering with respect to the elastic processes. In spite of this, a lidar with the capabilities of discriminate between inelastic (RAMAN) and elastic (MIE/Rayleigh) backscatter photons is a very powerful instrument for the observation of the aerosol optical properties (more details in the next paragraphs).

Figure I.3.14 shows the complete spectrum of the Raman backscattered photons; when the emitted ones are in the UV range (355-nm wavelength), for each specific molecule (N_2, O_2, and H_2O) the wavelength shift of the vibrational line and of the roto-vibrational wings is the signature of the molecule itself.

6 Aerosol-Devoted Lidar

I will discuss the main features of a simple lidar systems designed to measure the vertical profile of the aerosol extinction coefficient, $\alpha_{\text{aer}}^{\lambda_o}(s)$ and of the aerosol backscatter coefficient, $\beta_{\text{aer}}^{\lambda_o}(s)$. Their dependence from the aerosol optical and physical parameters is described by

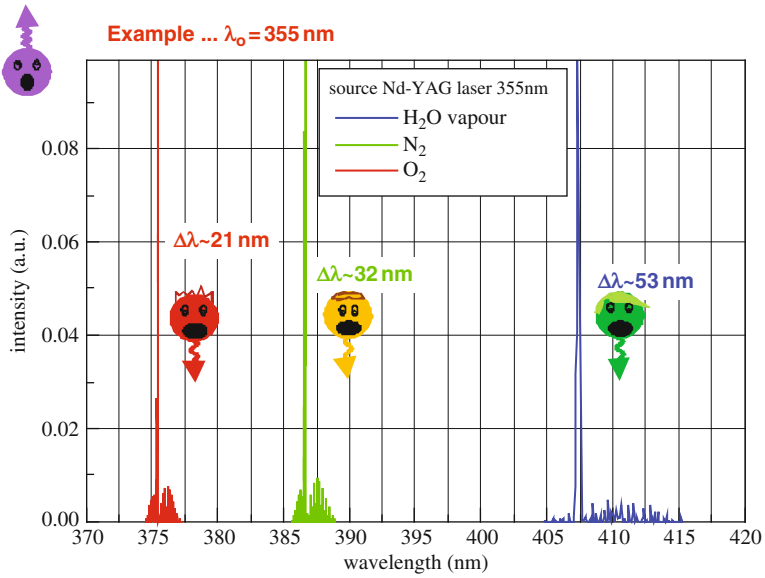

Fig. I.3.14 The Raman backscatter photons when the emitted wavelength is 355 nm (Nd-Yag laser-third harmonics)

$$\alpha_{\text{aer}}^{\lambda_o}(s) = \int_0^\infty dr\pi r^2 Q_{\text{ext}}(r, m, \lambda_o) n_{\text{aer}}(s, r) \tag{2}$$

and

$$\beta_{\text{aer}}^{\lambda_o}(s) = \int_0^\infty dr\pi r^2 Q_{\text{bck}}(r, m, \lambda_o) n_{\text{aer}}(s, r), \tag{3}$$

where $n_{\text{aer}}(s, r)$ is the aerosol size distribution, and $Q_{\text{ext}}(r, m, \lambda)$ and $Q_{\text{bck}}(r, m, \lambda)$ are the Mie extinction and backscattering efficiencies of an aerosol particle of radius r, index of refraction m, at wavelength λ.

6.1 Aerosol Raman Lidar

It should be said that the use of single wavelength (elastic) lidar suffers from the fact that two physical quantities, the aerosol backscatter and extinction coefficients, must be determined from only one measured lidar signal. This is not possible without assumptions about the relation between the two and estimate of a boundary or reference value of the aerosol extinction.

If we are able to detect the Raman backscattered photons, then the Raman return is more or less a direct measurement of the aerosol extinction (Fig. I.3.15).

The Raman lidar technique can provide unbiased measurements of the aerosol optical properties: extinction and backscatter coefficients (Ansmann et al., 1992),

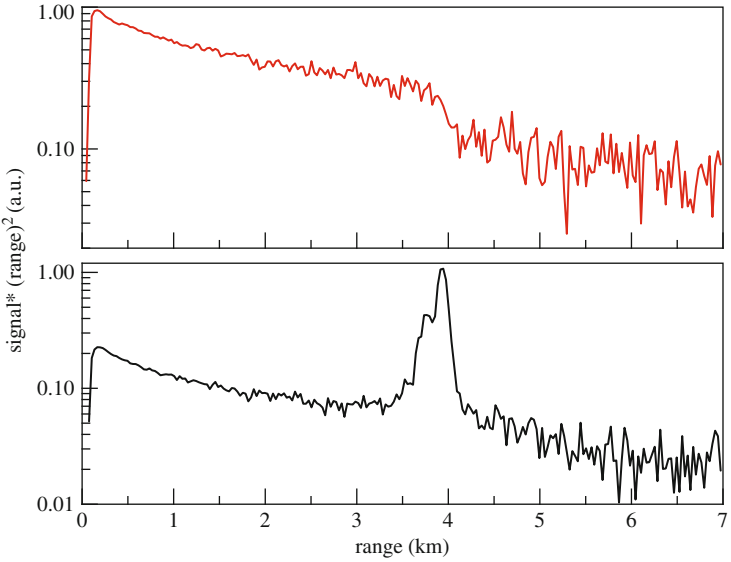

Fig. I.3.15 Raman lidar signal (*above*) and the elastic lidar backscatter (*below*) in the presence of cloud aerosols. Note the quite clear signature of the cloud transmission in the Raman return

both of them, straightforwardly used for the assessment of the atmospheric optical transmission, are indirect measurements of the aerosol concentration. For example, the analysis of the extinction and backscatter vertical structures gives information about the planetary boundary layer (Matthias and Bosenberg, 2002).

Rayleigh/Mie and Raman lidar inversion methods are well known (Ferrare et al., 1998), and it has been demonstrated that the combination of the different methods leads to an improvement of the results. With regard to these measurements, a complete description of algorithms and assessment of the data quality can be found in Bockmann et al. (2004) and Pappalardo et al. (2004).

The aerosol extinction can be determined from N_2 Raman lidar return through the application of the following expression:

$$\alpha_{\mathrm{aer}}^{\lambda_o}(s) = \frac{\frac{d}{dz}\left\{\ln\left[\frac{n_{\mathrm{mol}}(s)}{s^2 N_{\mathrm{R}}(s)}\right]\right\} - \alpha_{\mathrm{mol}}^{\lambda_o}(s) - \alpha_{\mathrm{mol}}^{\lambda_R}(s)}{1 + \left(\frac{\lambda_o}{\lambda_R}\right)^k}, \tag{4}$$

where $N_{\mathrm{R}}(s)$ is the Raman return at wavelength $\lambda_{\mathrm{R}} = (\lambda_o + \Delta\lambda_{N_2})$ [$\Delta\lambda_{N_2}$ is the Raman shift of N_2], $n_{\mathrm{mol}}(s)$ is the atmospheric molecular number density, $\alpha_{\mathrm{mol}}^{\lambda_o}(s)$ and $\alpha_{\mathrm{mol}}^{\lambda_R}(s)$ are the extinction coefficients due to absorption and Rayleigh scattering by atmospheric gases; the Mie aerosol scattering is assumed to be proportional to λ^{-k}. Then, it needs to evaluate a numerical derivative for the estimation of the aerosol extinction coefficient; both $\alpha_{\mathrm{aer}}^{\lambda_o}(s)$ and its uncertainty could be misevaluated if data acquisition and analysis are not correctly accomplished.

The uncertainties affecting $\alpha_{\mathrm{aer}}^{\lambda_o}(s)$ are mainly due to:

- the statistical error due to signal detection;
- the systematic error associated with the estimation of $n_{\mathrm{mol}}(s)$ (i.e., from pressure and temperature profiles);
- the systematic error associated with the evaluation of k, aerosol scattering wavelength dependence;
- the errors introduced by operational procedures such as signal binning (smoothing) and averaging (accumulating lidar returns);

The above expression for $\alpha_{\mathrm{aer}}^{\lambda_o}(s)$ can be applied to the altitude range where the lidar overlap is complete [$G(s) = 1$], otherwise an additional systematic error should be accounted for.

The aerosol backscattering coefficient is evaluated according to:

$$\beta_{\mathrm{aer}}^{\lambda_o}(s) = \beta_{\mathrm{mol}}^{\lambda_o}(s)\left[\frac{N(s)}{N_{\mathrm{R}}(s)} \cdot \frac{A_{\mathrm{R}}}{A_o} \cdot \frac{\sigma_{\mathrm{Raman}}^{\lambda_R}(\pi)\cdot f}{\sigma_{\mathrm{mol}}^{\lambda_o}(\pi)} \cdot \frac{T_{\mathrm{mol}}^{\lambda_R}(s)}{T_{\mathrm{mol}}^{\lambda_o}(s)} \frac{T_{aer}^{\lambda_R}(s)}{T_{\mathrm{aer}}^{\lambda_o}(s)} - 1\right], \quad (5)$$

where $N(s)$ is the Rayleigh/Mie elastic return, $T_{\mathrm{mol}}^{\lambda}(s)$ is the molecular transmission, $T_{\mathrm{aer}}^{\lambda}(s)$ is the aerosol transmission at wavelength λ; A_o and A_{R} account for the optical and electronic efficiencies of the corresponding lidar channel; $\sigma_{\mathrm{mol}}^{\lambda_o}(\pi)$ and $\sigma_{\mathrm{Raman}}^{\lambda_R}(\pi)$ are the differential backscattering cross section for Rayleigh and Raman molecular scattering; f is the volume mixing ration of N_2. The aerosol backscattering calculation needs to evaluate $\frac{A_{\mathrm{R}}}{A_o} \cdot \frac{\sigma_{\mathrm{Raman}}^{\lambda_R}(\pi)\cdot f}{\sigma_{\mathrm{mol}}^{\lambda_o}(\pi)}$, and this is done by imposing $\beta_{\mathrm{aer}}^{\lambda_o}(s) = 0$ in the range of altitude free of aerosols.

The uncertainties affecting $\beta_{\mathrm{aer}}^{\lambda_o}(s)$ are mainly due to:

- the statistical error due to signal detection;
- the systematic error associated with the estimation of $n_{\mathrm{mol}}(s)$ (i.e., from pressure and temperature profiles); and
- the errors introduced by operational (retrieval) procedures.

The design of the Raman lidar receiver (the telescope can be coupled to the detector box through an optical fiber) assigns the same overlap function to the Rayleigh/Mie elastic and N_2 Raman lidar channels; because the evaluation of $\beta_{\mathrm{aer}}^{\lambda_o}(s)$ involves the ratio between the two lidar returns, the retrieval procedure of the aerosol backscattering coefficient results independent of the lidar geometrical overlap.

Other quantities are usually evaluated: the vertical aerosol optical depth (VAOD) and the integrated aerosol backscatter coefficient (INTAβ) up to 4–5 km range, and, also, the *mean* lidar ratio (LR). The VAOD and INTAβ, between the range heights s_1 and s_2, are defined as

$$\mathrm{VAOD}(s_1, s_2) = \int_{s_1}^{s_2} \alpha_{\mathrm{aer}}^{\lambda_o}(s')ds', \tag{6}$$

$$\mathrm{INTA}\beta(s_1, s_2) = \int_{s_1}^{s_2} \beta_{\mathrm{aer}}^{\lambda_o}(s')ds'. \tag{7}$$

And, the *mean* LR is calculated according to

$$\mathrm{LR} \cong \frac{\mathrm{VAOD}(s_1, s_{\mathrm{PBL}})}{\mathrm{INTA}\ \beta(s_1, s_{\mathrm{PBL}})}. \tag{8}$$

Typically, $s_1 \cong 0.5$ km and $s_2 \cong 3 - 5$ km; below s_1 it is assumed that the extinction and backscatter coefficients are constants, $\alpha_{\mathrm{aer}}^{\lambda_o}(s_1)$ and $\beta_{\mathrm{aer}}^{\lambda_o}(s_1)$, respectively.

The evaluation of VAOD can be done directly from the N_2 Raman lidar return:

$$\mathrm{VAOD}(s_1, s_2) = -\frac{\ln\left(\frac{N_{\mathrm{R}}(s)s^2 n_{\mathrm{mol}}(s)}{T_{\mathrm{mol}}^{\lambda} T_{\mathrm{mol}}^{\lambda_o}}\right)}{1 + \left(\lambda_o/\lambda\right)^k} + C. \tag{9}$$

6.2 Lidar Setup

The typical setup of a Raman lidar is shown in Figure I.3.16 (L'Aquila Raman lidar).

The laser, telescope, and a receiver are designed to discriminate among the different Raman backscattered photons (Fig. I.3.17). A possible but not easy task! ... choosing and combining optics and spectrometer-wise components, the efficiencies in collecting photons of the various detectors look like those reported in Fig. I.3.18.

In summary the main characteristics of a Raman lidar are:

- capability of detecting low light levels,
- suppression of cross-talking between the different channels (i.e., suppression of the strong elastically backscattered light in Raman channels), and
- range-independent collecting efficiencies.

7 Raman Lidar Aerosol Observations

The $\alpha_{\mathrm{aer}}^{\lambda_o}(s)$ and $\beta_{\mathrm{aer}}^{\lambda_o}(s)$, reported in Fig. I.3.19, represent the typical products obtained from a single measurement session of the L'Aquila Raman lidar.

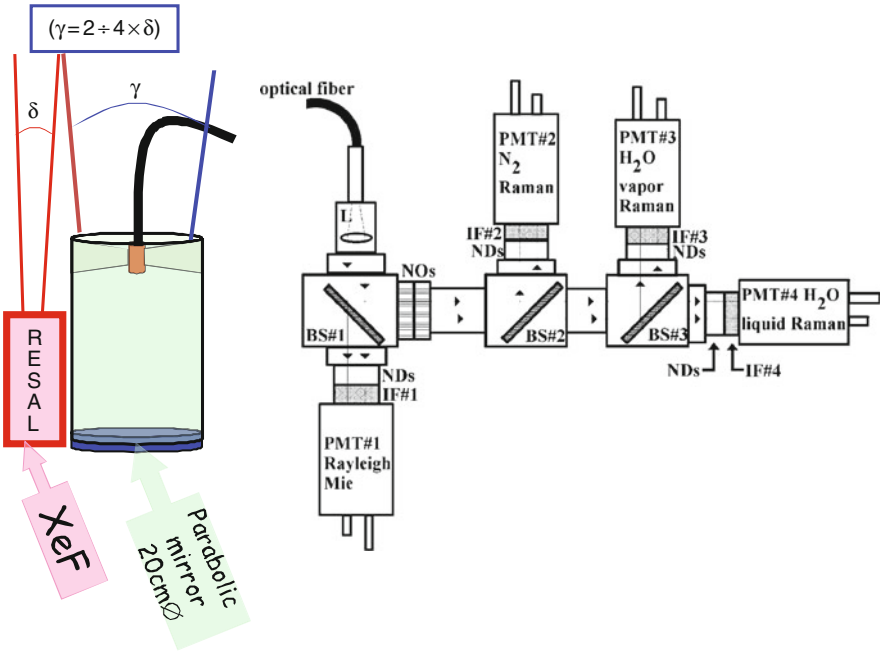

Fig. I.3.16 UV Raman lidar L'Aquila. In the optical layout of the receiver's beam separator, L is a 1-inch plano-convex lens, BS indicates dichroic beam splitters, IF, ND, NO, and PMT labels 2-inch interference filters, the interchangeable neutral density filters, the notch filters, and the photomultipliers, respectively. The spectral features of each channel are indicated by a representative wavelength: 351 nm – Rayleigh/Mie channel, 382 nm – Nitrogen Raman channel, 393 nm – liquid water Raman channel, 403 nm – water vapor Raman channel

As cited, other quantities are usually evaluated: the vertical aerosol optical depth (VAOD) and the integrated aerosol backscatter coefficient (INTAβ) up to 4–5 km range, and, also, the *mean* lidar ratio (LR). In addition, from the analysis of the single aerosol backscatter profile it is possible to estimate the boundary layer height (s_{PBL}).

How to retrieve (practically) this data from the lidar returns will be discussed in the next paragraphs.

7.1 Backscatter and Extinction

The quantities measured by the lidar contain information about the aerosol composition (Q's) and size distribution (n_{aer}).

$$\alpha^{\lambda}_{\mathrm{aer}}(s) = \int_0^{\infty} dr.\pi r^2 \cdot Q_{\mathrm{ext}}(r, m, \lambda) \cdot n_{\mathrm{aer}}(s, r)$$

$$\beta^{\lambda}_{\mathrm{aer}}(s) = \frac{1}{4\pi} \int_0^{\infty} dr \cdot \pi r^2 \cdot Q_{\mathrm{bck}}(r, m, \lambda) \cdot n_{\mathrm{aer}}(s, r)$$

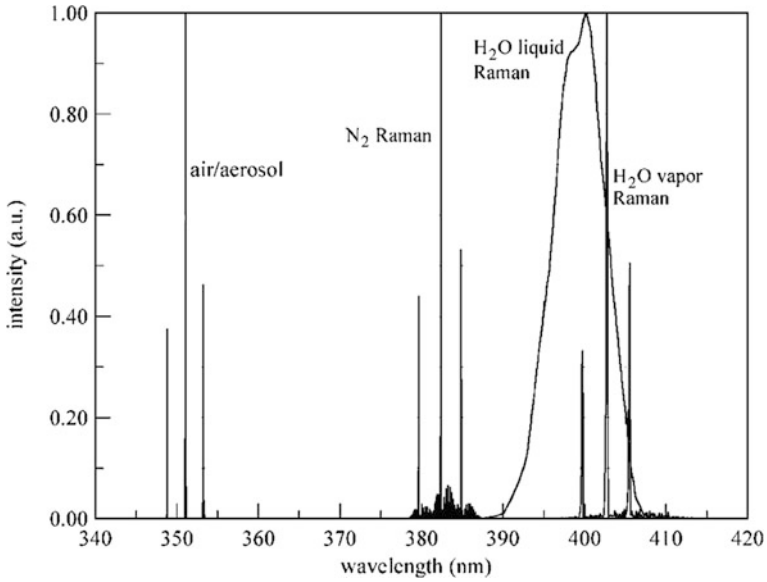

Fig. I.3.17 Schematic drawing of the Rayleigh/Mie and Raman components of the return light spectrum. The Rayleigh/Mie part is a reply of the laser spectrum that has been measured; the different Raman bands have been plotted on wavelength scale, again give a look to the spectrum of the backscattered photons, elastic and inelastic ones. Three spectral lines are for each band, because the emitted photons are distributed over three laser lines (XeF excimer laser)

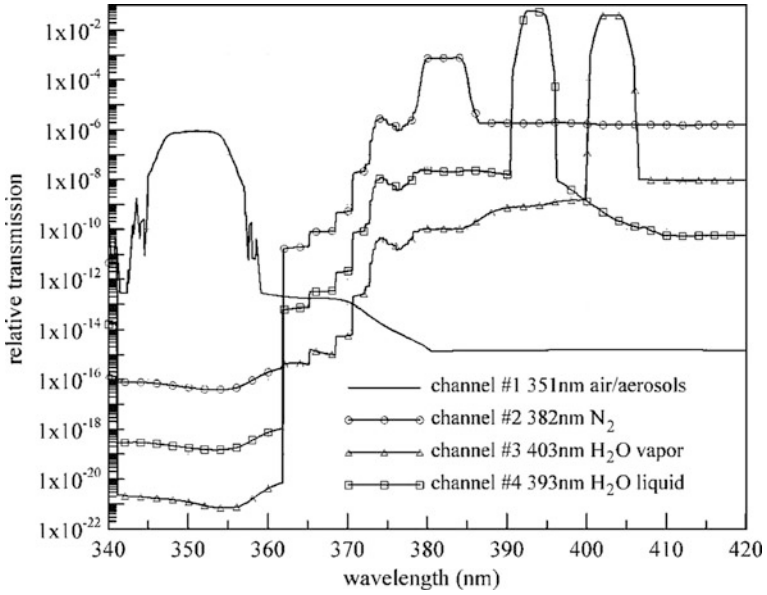

Fig. I.3.18 The wavelength-dependent relative transmissions of the beam separator. These curves have been estimated using the manufacturer's data sheet and the specifications of the various components (filters, mirror, lenses, optical fiber, etc.)

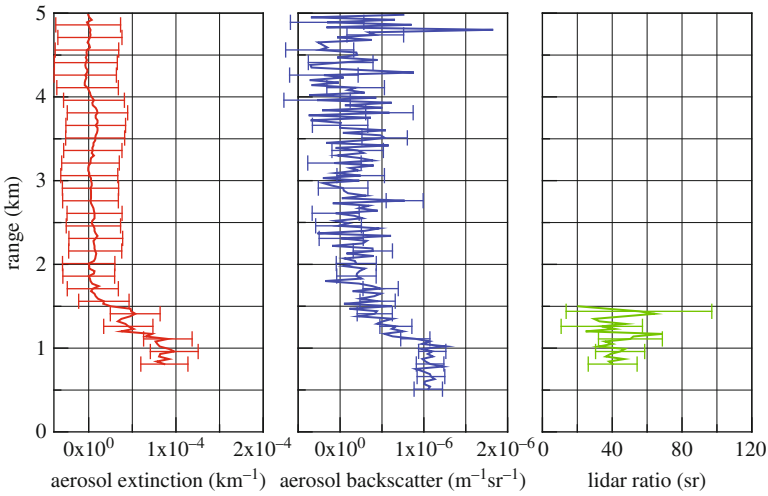

Fig. I.3.19 Typical aerosol extinction, backscatter, and lidar ratio profiles measured by the L'Aquila Raman lidar. The error bars indicate the propagated statistical indetermination

Let us give a look to a couple of (numerical) examples: sulfate aerosols and the cloud droplets (as produced by a cloud model).

7.2 Sulfate Aerosols and Cloud Droplets

Scattering and extinction efficiencies (Q's in Fig. I.3.20) can be estimated using well-known theories (Mie, 1908), but they also have a very complicate dependence on aerosol size and composition. Size distribution is in such a case log-normal (Fig. I.3.21).

In *cloud case*: $\alpha_{\text{aer}}^{\lambda_0}(s) = 0.023\ \text{m}^{-1}$ and $\beta_{\text{aer}}^{\lambda_0}(s) = 0.0015\ \text{m}^{-1}\text{sr}^{-1}$, it is a quite dense cloud; roughly, the visibility is less than 200 m.

A Raman lidar measures the vertical profile of these quantities at quite fast rates. It could be realized how powerful could be the lidar technique, if applied at different wavelengths. It is possible to measure the aerosol backscattering and extinction in a range of wavelengths, and from these information it is possible to estimate (with a certain precision) the aerosol composition and size distribution.

8 Lidar Signal Simulator

As promise some examples down- and upsizing the different lidar components (using a LIdar Signal Simulator program LISISI, available at vincenzo.rizi@aquila.infn.it) for evaluating the better configuration of the lidar system

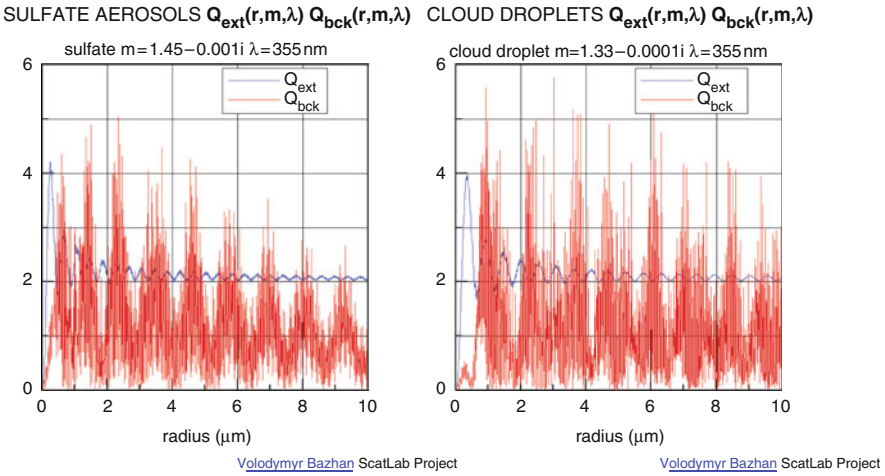

Fig. I.3.20 The scattering and extinction efficiencies vs aerosol dimensions for the case of sulfate aerosol and water cloud droplets (Volodymyr Bazhan, ScatLab Project)

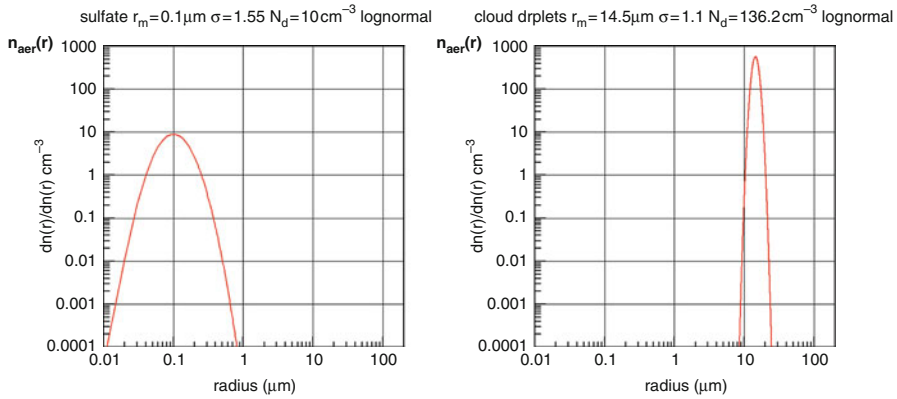

Fig. I.3.21 The typical size distributions of sulfate aerosols and cloud water droplets

in various situation: measuring the aerosol optical properties in the boundary layer or in the case of low-/high-level clouds.

We can also play in figuring out what happens in the case of simple technical variation of the setup (telescope collecting area, laser energy, increasing of the noise, etc.) (Fig. I.3.22).

Example of lidar configuration to be use with LISISI:

ELASTIC LIDAR clean (free of aerosol) atmosphere

	Laser energy (mJ)	Telescope radius (m)	No. laser shots	eff.	Background	Aerosol
Case 1	5 (355 nm)	0.1	18,000	2e-8	1	NO
More background (daytime!)						
Case 2	5(355 nm)	0.1	18,000	2e-8	10	NO
Weaker laser						
Case 3	1(355 nm)	0.1	18,000	2e-8	1	NO
Smaller telescope						
Case 4	5(355 nm)	0.05	18,000	2e-8	1	NO

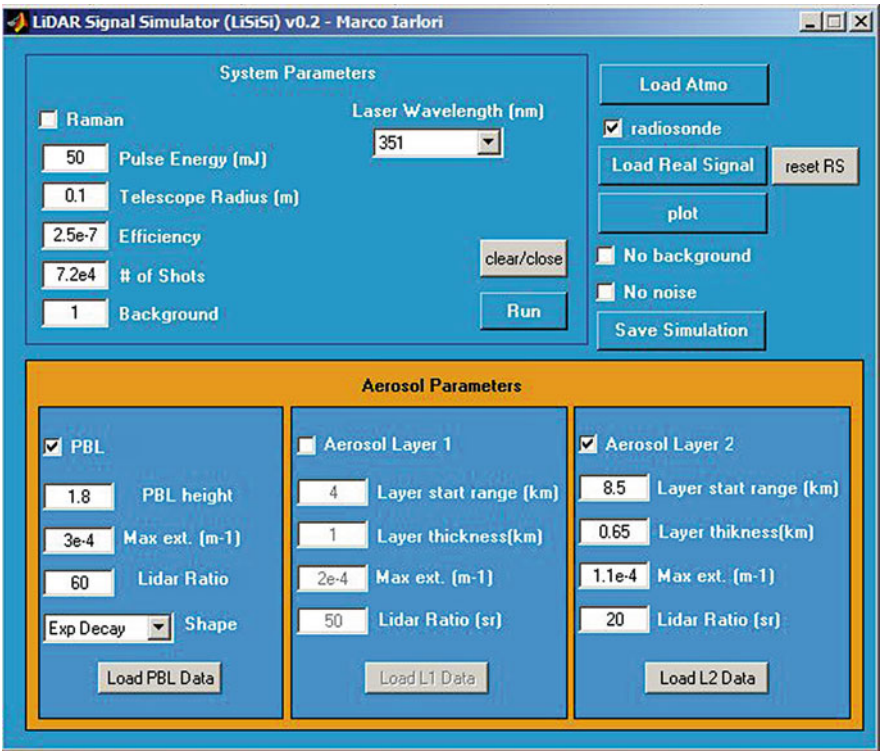

Fig. I.3.22 The user interface of lidar signal simulator. It is possible to set different parameters of the lidar system and of the simulated atmosphere

The evidence is that in cases 2 (higher noise), 3 (lower laser energy) and 4 (smaller telescope), the sampling of the atmosphere is less efficient.

Let us introduce some aerosol (cirrus) a 1-km thick cloud at 10-km range, optical depth of about 0.2, with the parameters of case 1. It happens that the lidar sounding does not show a clear signature of the cloud. What could we do?

Should we buy a more powerful laser, a larger telescope, or better optics? . . . If no money?

Increase the accumulation of laser shots!

ELASTIC/Raman LIDAR atmosphere with aerosols

	Laser energy (mJ)	Telescope radius (m)		No. laser shots	eff.	Background	aerosol
Case 5	5 (355 nm)	0.1	72,000	2e-8	1	cirrus	
Let me set a reference for elastic case (our system!):							
Case 6	50 (355 nm)	0.1	72,000	2e-8	1	cirrus	
And try to change the wavelength . . . from UV to a visible laser							
Case 7	50 (532 nm)	0.1	72,000	2e-8	1	cirrus	
The backscatter sign apparently increases! More information?							
And try to give a look to the Raman return							
Case 8	50	0.1	72,000	2e-4*	1	cirrus	Ram
It evident the effect of the extinction within the cloud							
Finally, we try to see what should be the effect of the aerosol in PBL (constant content in PBL and exp. decay in free troposphere) into the lidar returns.							
Case 9	50	0.1	72,000	2e-8	1	PBL	
Case 10	50	0.1	72,000	2e-4*	1	PBL	Ram

It is evident that the signature of such aerosol load is very weak and, in the next paragraph, I will show how from these signals it is possible to estimate the aerosol optical properties with the appropriate error bars.

Finally, such kind of virtual instrument is very useful for designing the system and planning the observations.

The main task of this part of the lecture is to give an idea of how the aerosol lidar returns can be analyzed to estimate some aerosol optical properties (namely, aerosol backscatter and extinction coefficients). We will play again with some software; hopefully it will be clear how much significant the aerosol lidar products are. This is the expected outcome: have clear the main features concerning the quality and the significance of lidar measurements.

9 Lidar Signal Analysis

Let me refer to a real system (L'Aquila Raman lidar discussed in paragraph 6.2). As first step we can play with the lidar signal simulator for the best fitting to the real signal changing the aerosol content in the simulated atmosphere. It is nice, but we cannot get quantitative information (Fig. I.3.23).

To be more quantitative, from the elastic and N_2 Raman signals it is possible to evaluate the aerosol backscattering coefficient and vertical aerosol optical depth (the cumulative integral of the extinction coefficient). To do this you should have information about the molecular part of the atmosphere (pressure and temperature profiles), and you can use Eqs. (5) and (8), together with some, very common,

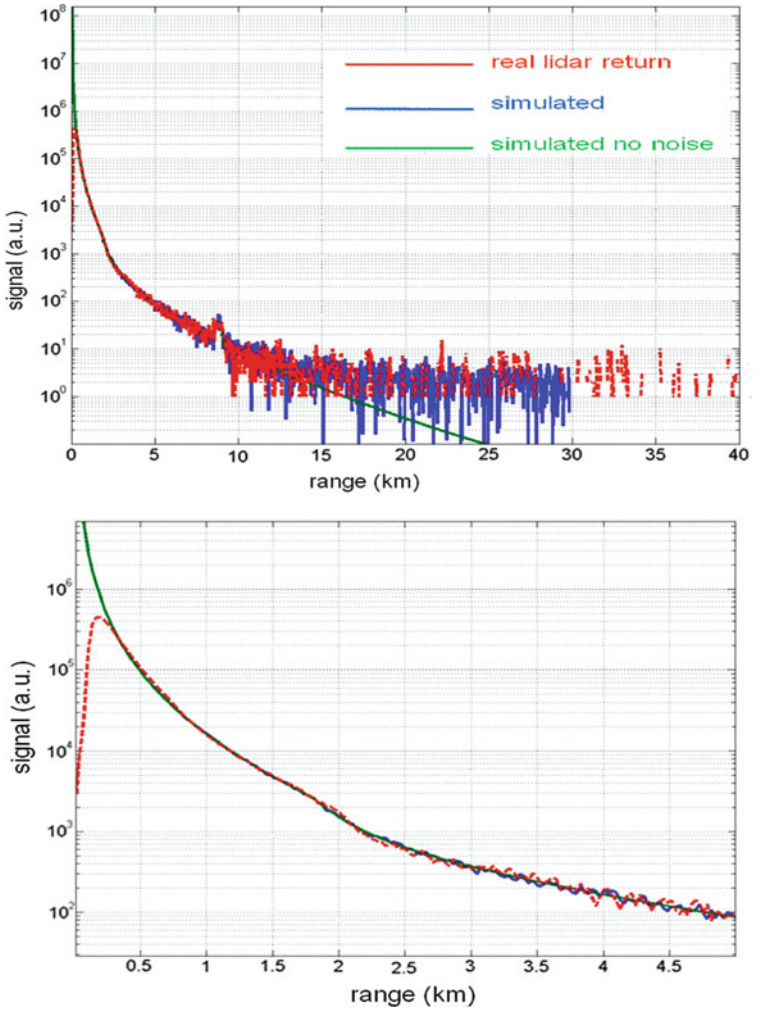

Fig. I.3.23 Real lidar signals (elastic – *upper panel*, Raman – *lower panel*) and simulated returns

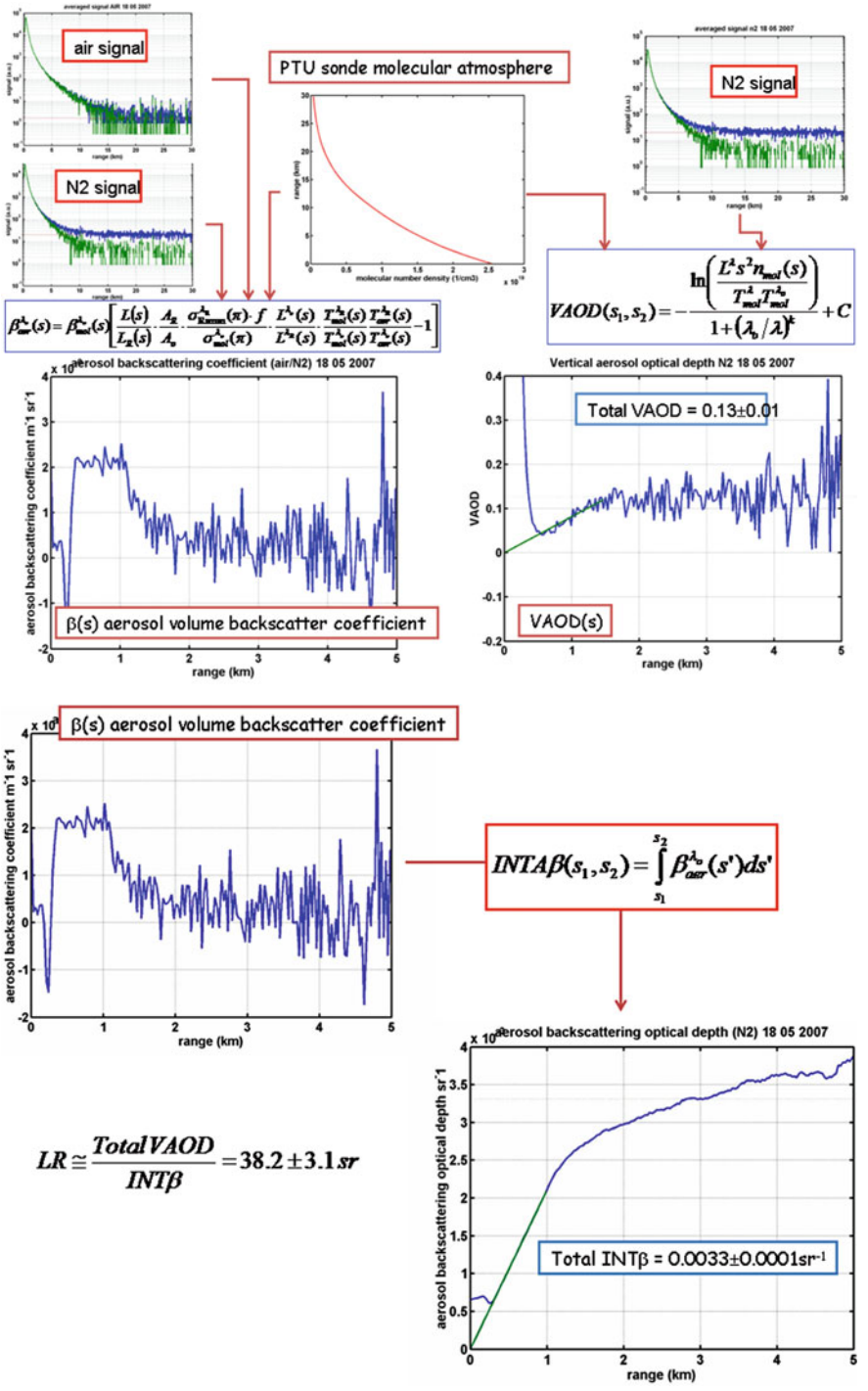

Fig. I.3.24 Procedure for the evaluation of VAOD and aerosol backscatter coefficient profiles, the integrated aerosol backscatter, and the mean lidar ratio

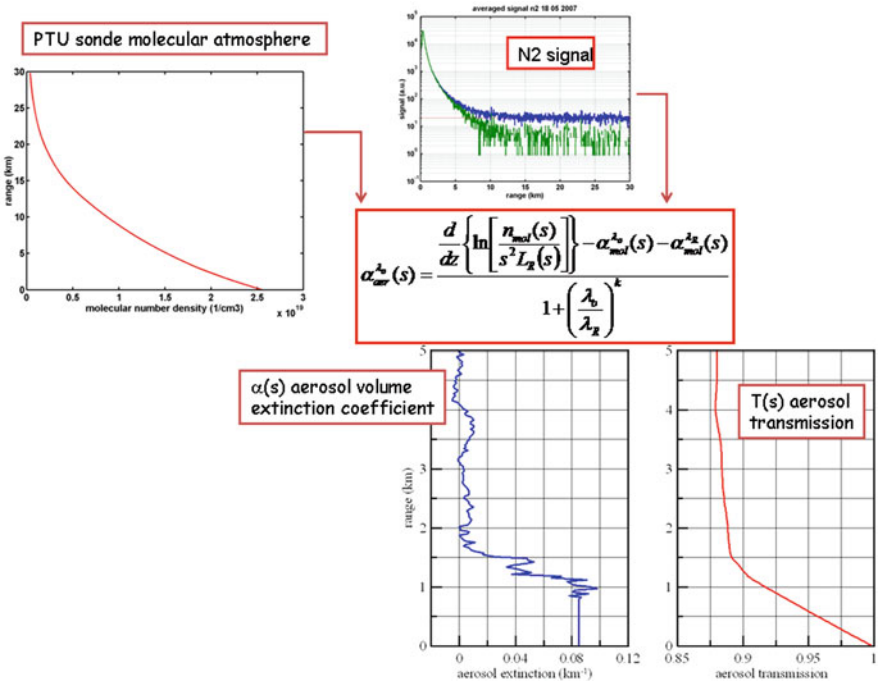

Fig. I.3.25 Procedure for the evaluation of aerosol extinction coefficient profile

numerical filters. After this procedure you can estimate (in this case) the total vertical aerosol optical depth with an indetermination less than 10% (the overall algorithm is reported in Fig. I.3.24).

For another interesting quantity (the vertical profile of the aerosol extinction coefficient) there is a different story, you should apply more sophisticated numerical filters, and their features have a direct effect on the indetermination to be assigned at the observations (Fig. I.3.25).

This Raman aerosol lidar produces such kind of results along 40-min measurement session. Note the typical structure of the aerosol vertical distribution: constant along the PBL (0–1 km range) and decaying faster in the free troposphere (above 1 km range).

10 Aerosol Observation

In this section, I report an example of extensive aerosol observations, and this concludes the lectures.

These aerosol measurements have been taken by a lidar used for the purposes of an ultra high energy cosmic ray experiment (Pierre Auger Observatory, http://www.auger.org/, which is located in Argentina). This experiment studies the

cosmic rays at very high energies and uses the atmosphere as a calorimeter. To evaluate the cosmic ray energy, among the other properties, the optical transmission of the atmosphere should be known. The portion of this transmission due to the presence of the aerosol is the most variable components (this is the point of view of a cosmic ray physicist!). The Raman lidar is the right instrument for monitoring such properties! Using resources from different agencies ... a simple Raman lidar has been funded ... and for about 1 year has taken measurements.

The measurements have been carried on by the AUGER Raman Lidar from August 2006 to July 2007 at Los Leones (35.32 S, 69.30 W, 1,416 m a.s.l., Malargue, Mendoza, Argentina), and they constitute a year-round database of aerosol backscatter and extinction profiles in the UV range. The aerosol observations are presented and discussed, mainly, for assessing their scientific usefulness.

The AUGER Raman lidar is remotely operated. A Nd-YAG laser is the source of the laser pulses (third harmonics of fundamental wavelength: $\lambda_o = 355$ nm) and the backscattered light is collected by an *f*/3 parabolic Ø50 cm mirror that is coupled with an optical fiber to the receiver. The receiver box is set up with dichroic beam splitters, interference filters, and photomultipliers for discriminating (detecting) between the Rayleigh/Mie and Raman backscattered photons. The receiver optics and the data acquisition system have been extensively tested and characterized; a discussion of the technical details and the performances/limitations of the system can be found in Rizi et al. (2006). In summary, the AUGER Raman lidar has the needed spectral performances for an efficient separation between the detection of elastic (Rayleigh/Mie scattering by air molecules and aerosols) and of the weak wavelength-shifted Raman lidar returns (N_2 Raman scattering). The system can measure, with good precision, aerosol extinction and backscatter coefficients accumulating lidar returns for about 40 min (≈48,000 laser shots at 20 Hz laser pulse repetition rate). The aerosol data profiles can be usefully measured along a height range (i.e., altitude above the lidar) spanning from ≈500 m (below the lidar returns are modulated by the range-dependent geometrical overlap function, $G(s)$, that depends on the laser divergence, the receiver field of view, and the distance between telescope and laser axes; and it is a measure of the collecting efficiency of the receiver telescope) up to 5–7 km; the raw altitude resolution is 30 m.

The main results of 1-year measurements are summarized in Figs. I.3.26–I.3.28.

The PBL thickness (s_{PBL}) shows low values in fall/winter and enlarges in spring/summer. The extension of the entrainment region (h) is reduced during late spring/summer, this means that the free troposphere is more stable than in autumn/winter, and the vertical mixing is damped (Note that the lidar is operating in the austral hemisphere, i.e., winter is between the month 6–9).

The annual cycle of the aerosol optical properties is quite evident.

The Raman (monthly mean) VAODs and INTAβ show:

- low values during late fall and early winter,
- high values in summer, and
- relative high content of aerosol in late winter and early spring (is it a diffuse regional meteorological pattern? Do the occurrences of dust storms increase?)

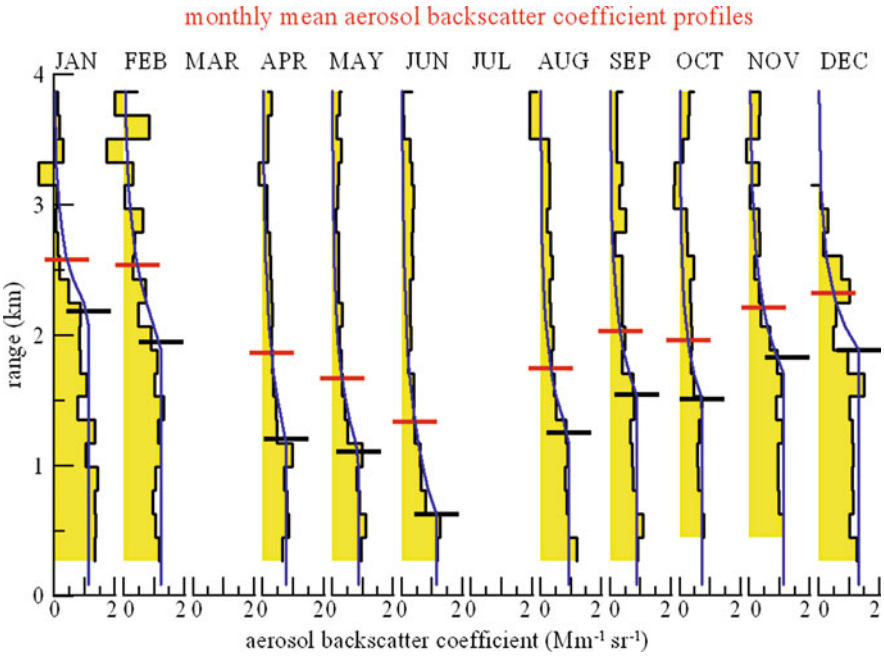

Fig. I.3.26 Monthly mean aerosol backscatter coefficient profiles; the horizontal ticks indicate the positions of the planetary boundary layer (PBL) upper levels and of the extensions of the entrainment zone above PBL over the lidar site

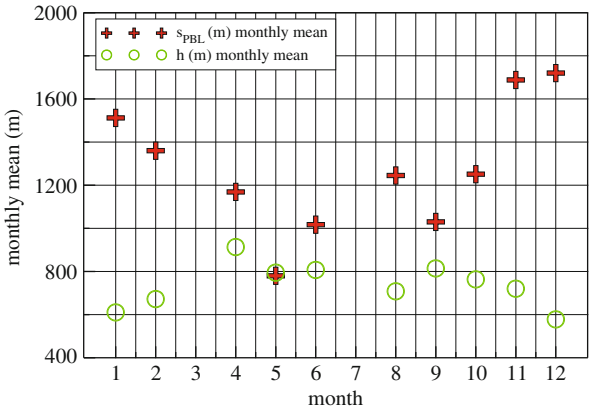

Fig. I.3.27 Monthly mean values of the PBL thickness (s_{PBL}) and the extension of the entrainment region (h)

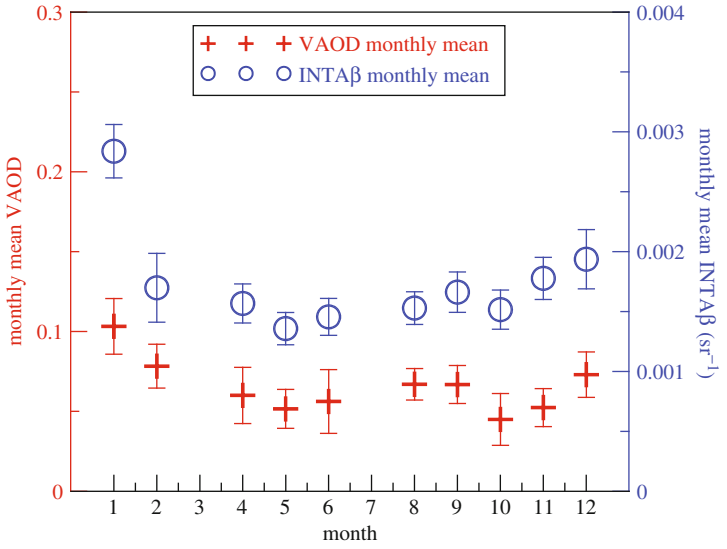

Fig. I.3.28 Monthly mean values of VAOD, INTAβ. The error bars indicate the corresponding standard deviations

References

Ansmann A et al. (1992) Combined Raman elastic-backscatter lidar for vertical profiling of moisture, aerosol extinction, backscatter, and lidar ratio. Appl Phys B 55:18–28.

Bockmann C et al. (2004) Aerosol lidar intercomparison in the framework of the EARLINET project. 2. Aerosol backscatter algorithms. Appl Opt 43:977–989.

Eltermann L (1951) The measurement of stratospheric density distribution with the searchlight technique. J Geophys Res 56:509–520.

Ferrare RA et al. (1998) Raman lidar measurements of aerosol extinction and backscattering, 1, methods and comparisons. J Geophys Res 103:19663–19672.

Fiocco G, Smullin LD (1963) Detection of scattering layers in upper atmosphere. Nature 199:1275–1276.

Hulburt EO (1937) Observations of a searchlight beam to an altitude of 28 kilometers. J Opt Soc Am 27:377–382.

Johnson EA et al (1939) The measurement of light scattered by the upper atmosphere from a search-light beam. J Opt Soc Am 29:512–517.

Ligda MGH (1963) Meteorological observations with a pulsed laser radar. In: Proceedings of the first conference on laser techniques, San Diego, CA, pp 63–72.

Maiman TH (1960) Optical and microwave-optical experiments in ruby. Phys Rev Lett 4:564–566.

Matthias V, Bosenberg J (2002) Aerosol climatology for the planetary boundary layer derived from regular lidar measurements. Atm Res 63:221–245.

McClung FJ, Hellwarth RW (1962) Giant optical pulsations from ruby. J Appl Phys 33:828–829.

Mie G (1908) Beiträge zur Optik trüber Medien speziell kolloidaler Goldlösungen. Ann Phys 25:377–445.

Pappalardo G et al. (2004) Aerosol lidar intercomparison in the framework of the EARLINET project. 3. Raman lidar algorithm for aerosol extinction, backscatter, and lidar ratio. Appl Opt 43:5370–5385.

Rizi V et al. (2006) The Raman lidar receiver at Pierre Auger Observatory: installation and hardware tests, GAP note 2006-015. Available at vincenzo.rizi@aquila.infn.it.
Schawlow AL, Townes CH (1958) Infrared and optical masers. Phys Rev 112:1940–1949.
Tuve MA et al. (1935) A new experimental method for study of the upper atmosphere. Phys Rev 48(11):917–918.